

A Study on the Influence of Cutting Tool Geometry on the Temperature of the Workpiece in Nanometric Cutting of Silicon



Prateek Gupta and Janakrajan Ramkumar

1 Introduction

Silicon is the backbone of the semiconductor industry. Apart from building transistors for electronics, the optical properties of single-crystal silicon make it one of the most suited choices for developing infrared light-based devices. Therefore, manufacturing techniques are required which can machine silicon with nanometric accuracy. The development of several techniques such as electron beam lithography (EBL), focused ion beam (FIB) milling [1] and femtosecond laser machining [2] has opened up a new research field known as ultra-precision machining. The modeling of these processes at a nanometric scale possess a challenge due to the breakdown of the assumption of the continuum and this is where molecular dynamic simulations (MDS) provide a solution. Several software tools that use this technique have come up in the last decade. These tools include GROMACS [3], AMBER [4], DL-POLY [5] and LAMMPS [6]. Different tools have a different user community and are often specialized for a specific type of research. In this work, we have used LAMMPS as the primary tool of analysis.

Single-point diamond turning (SPDT) is a promising approach for the fabrication of micro/nanostructures by machining the desired structure directly on the surface of the workpiece. Using a single-point diamond turning tool [2] to remove material to obtain flat surface up to a certain surface roughness [7–9]. SPDT gives mirror-finish on most materials and is preferred over other ultra-precision manufacturing methods. Silicon is the backbone of the semiconductor industry [10]. Almost all the electronic devices in use today employ at least some kind of silicon-based semiconductors.

P. Gupta (✉) · J. Ramkumar
Indian Institute of Technology, Kanpur 208016, India
e-mail: ptkiitk@gmail.com

J. Ramkumar
e-mail: jrkumar@iitk.ac.in

SPDT was invented in the 1980s to obtain the desired surface finish on silicon. Such precision is required in applications, where the optical properties of silicon have a considerable role to play, for example, infrared light-based devices and has the potential to reduce the size of transistors which has been a constant source of progress in the electronics industry. Moore's law is the observation that the number of transistors in a dense integrated circuit (IC) doubles about every two years. However, it has been estimated that Moore's law would no longer be valid by 2025 since the development of technology to reduce the size of transistors is not progressing at the required rate [11].

Several studies have used MD simulations to study the nanometric cutting process for different material-tool combinations. The studies use different types of inter-atomic potentials, temperature conditions, software and models. LAMMPS is most extensively used for the simulation of nanometric cutting.

In work presented by Goel et al. [9], MDS performed using LAMMPS was used to simulate SPDT. The work aimed at investigating the wear of the diamond tool for different crystal orientations. ABOP potential functions were used. Results showed the strong influence of crystal orientation on the wear resistance of a diamond tool. The formation of SiC due to the high temperature, and pressure due to high-pressure phase transformation (HPPT) was also observed.

An essential contribution in the field of nanometric cutting was made by Goel et al. [8]. In this work, the mechanism of wear for the diamond tool in nanometric cutting of silicon was presented. The study found the formation of *SiC* on the surface of the workpiece and the tool. This was also explained using the stress and the radial distribution of silicon carbide concerning simulation time. The work was in excellent agreement with experimental data obtained through the X-ray photoelectron spectroscopy and the stresses involved in the simulation, and the stress data obtained in the simulations.

In work reported by Cai et al. [12], a new silicon cutting mechanism at the nanoscale was presented. The study used LAMMPS as the software tool for the simulation, and an infinitely hard tool was modeled. Tersoff potentials were used to model the interactions. The forces and the stresses during the cutting process were observed. The study focused on crack formation during the cutting process and the mode of failure during the cut that leads to chip formation. The study also investigated the effects of various deformed/undeformed chip thickness ratios and the corresponding mechanism of cutting.

In Zhang et al. [13], nanometric cutting of copper was studied in terms of the subsurface damage caused by the cutting process at different depths of cut and at different cutting speeds. The deformations of the crystal structure of copper was reported. It was reported that the cutting speed of the process makes little difference to the proportion of the BCC atoms in the region of cut. The different types of dislocation observed with different cutting depths was also reported.

In work reported by Fang et al. [14], nanometric cutting of monocrystalline silicon was simulated. The study aimed to identify the mechanism of chip formation in the cutting process and presented a model that used extrusion to explain chip formation instead of shearing used in conventional machining. Nanoindentation experiments

were found to be in good agreement with the simulation data. Tersoff potentials were used to model the interaction between the atoms, and the tool was assumed to be infinitely hard.

In a work presented by Kalkhoran et al. [15], nanometric cutting using a blunt tool was studied. A parameter called relative tool sharpness (RTS), defined as the ratio of undeformed chip thickness and tool radius, was used to characterize the cutting process. The cutting process was simulated using LAMMPS. The machining forces for different RTS were reported, along with the force ratios and the effective tool rake angles. The study used an infinitely hard tool, and the workpiece was modeled as single-crystal silicon. Tersoff potentials were used to model the interactions between different atoms.

In the work presented by Lie et al. [16], molecular dynamic simulations were performed using a grooved diamond cutting tools were used to manufacture structures on a silicon workpiece. ABOP potentials were used to model the interactions between the atoms. The cutting forces on the tool and workpiece along with the temperature distribution of the tool were reported. The geometry of the groove was varied, and the tool was assumed to be blunt or the study.

In the study by Lianfenga et al. [17], the effect of tool radius was studied on the cutting of skiving monocrystalline silicon was studied using molecular dynamic simulations. The work studied the mechanisms of cut for the material with different roundness of the tool and concluded that while in the case of a sharp tool, the mechanism of material removal is predominantly shear, as the roundness of the tool increases, the mechanism of cut tends to move toward extrusion accompanied by shearing. However, for the purposes of this study, the tool has been assumed to be sharp.

In this study, the process of cutting monocrystalline silicon using single-point diamond cutting tools has been studied at nanometric scale using molecular dynamic simulations. In this work, process of nanometric cutting has been simulated, and the temperature of the region of cut has been observed. The forces on the tool have also been reported. The simulations have been run for different depths of cut and tools including positive and negative rake angle tools. A brief mathematical overview of MDS has been discussed in Sect. 2. The various parameters used for modeling the process and the respective configurations have been discussed in Sect. 3. The results have been discussed in Sect. 4. The conclusions of this work have been discussed in Sect. 5.

2 MD Simulation

MDS provides the numerical solution of Newton's laws of motion for an ensemble of atoms [18]. It is used to observe phenomena at very small-time steps ($10^{-10}s$) and at an enhanced resolution. MDS uses the position, velocity and acceleration of various atoms in the system under consideration to calculate the desired properties of the system. The atoms/molecules in MDS are modeled as individual spring mass

systems with a dynamic spring constant. These spring constants are modeled using the potential functions. The choice of potential function is an essential part of any MDS study since it is the primary bridge between the simulation and real-world interaction between the atomic entities. The potential functions and the parameters of these functions are selected such that they satisfy the basic physical properties of the system, and the model is stable. There are several different potential functions used to model different types of systems. These potential functions include Lennard–Jones (LJ) potentials [19], analytical bond-order potential (ABOP) [20], Morse potentials [21] and pair-wise Morse potentials, embedded atom model (EAM) potentials [22], Bolding-Anderson potential and Tersoff potentials [23, 24] each of which has its own merits and demerits. In most of these potential functions, the distance between two atoms is used as an input, and the potential energy of the two atoms due to their proximity with each other is calculated.

In MDS, the motion of atomic bodies is realized by calculating the resultant forces for each atom and integrating them to calculate their trajectory according to the Newton's laws of motion [25]. This is mathematically described in Eq. (1):

$$m \frac{d^2 r_i}{dt^2} = \frac{d(mv_i)}{dt} = \frac{dp_i}{dt} = F_i \quad (1)$$

where m is the mass of the atom and r_i , v_i , p_i and F_i are the position vector, velocity vector, momentum vector and the force acting on the i th atom, respectively. t is the time in the simulation at which the position, velocity and acceleration of the atoms are calculated. F_i is calculated as the gradient of the potential energy (PE) with respect to the position of the i th atom as given in Eq. (2):

$$F_i = -\nabla_i V(r_1, r_2, r_3, \dots, r_N) \quad (2)$$

where V is the potential energy function. N is the number of atoms and ∇_i is the gradient operator for the i th atom $\nabla_i = \frac{\partial}{\partial x_i} \hat{i} + \frac{\partial}{\partial y_i} \hat{j} + \frac{\partial}{\partial z_i} \hat{k}$. Each time, step of MD simulation has a length of the order of femtoseconds. It should be noted that if the number of atoms in the system is N , then the number of differential equations solved in each time step is $6N$, and hence, the process is computationally expensive, thus the need for the high-performance computational resources for such a study [25].

For each time step, the force on each atom is calculated, and the force is then integrated to obtain the displacement of the atoms. There are a few algorithms that are most commonly used for this integration, e.g., Leapfrog integration [26] and Verlet integration [27].

The velocity of the atoms is also used to calculate the temperature of a given region in the simulation box. This is accomplished by using the relationship between the kinetic energy of the atoms, and the temperature is obtained from the kinetic theory of gases in Eq. (3) [9].

$$\frac{1}{2} \sum_i m_i |v_i|^2 = \frac{3}{2} N k_b T \tag{3}$$

where k_b is the Boltzmann constant ($1.3806503 \times 10^{-23} \text{ J/K}$) and T is the atomistic temperature.

3 Modeling

Several methods for modeling this process have been mentioned in the literature, which differ in the use of potential functions, boundary conditions, parameters of the tool (for example, tool radius, rigid tool, deformable tool) and the nature of the atoms used. In this work, Tersoff potentials have been used to model the behavior of silicon atoms and their interaction with carbon atoms in the diamond tool. The parameters for Tersoff potentials are readily available in LAMMPS [23, 24]. The time step for the simulation has been kept at 0.5 fs. Figure 1 shows a schematic diagram of the simulated system. The details of the simulation parameters are given in Table 1. The movement of the workpiece is constrained on one side by a group of rigidly fixed atoms and unconstrained on the other side. This has been described by Komanduri et al. as an elastic boundary condition [25]. A description of the four types of atoms used in this study is given as follows.

1. Boundary atoms: These atoms have been fixed and modeled as perfectly rigid to simulate the bulk of the workpiece away from the cut region.
2. Peripheral atoms: These atoms have been used to simulate the thermodynamics of the system. NVT ensemble has been used to simulate these atoms. This is used

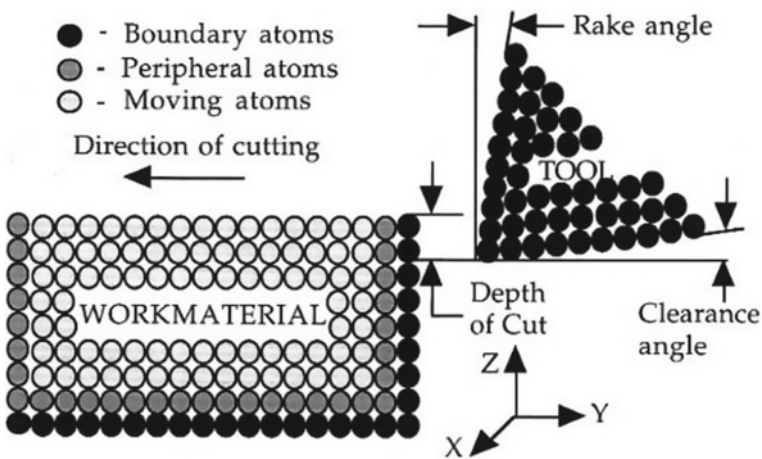


Fig. 1 Diagram of the atomic system studied

Table 1 Parameters used in the simulation with the lattice parameters of silicon $a = 5.431 \text{ \AA}$

Parameter	Value
Configuration	3D
Potentials used	Tersoff
Work material	Single-crystal silicon (diamond cubic)
Tool material	Perfectly rigid
Lattice parameter of workpiece	$a = 5.431 \text{ \AA}$
Velocity of cut	10 m/s
Relief angle	15°
Rake angle	$-30^\circ, -15^\circ, 0^\circ, 15^\circ, 30^\circ$
Depth of cut (DOC)	0a, 1a, 2a, 5a, 10a
Width of cut	5a
Dimensions of workpiece	$5a \times 70a \times 50a$

to simulate heat transfer in the system from the region of cut to the bulk of the workpiece. This layer has been kept to 2–3 atom thick as done in literature [25].

3. Tool atoms: The tool has been modeled to be rigid and sharp, the rake angle has been varied, and the tool velocity has been kept constant.
4. Workpiece atoms: These are atoms that have been modeled as following Newtonian physics. These atoms can be displaced and oscillate about their mean positions as dictated by Eq. (1).

4 Results and Discussion

All the simulations in this work have been performed using LAMMPS [6]. The data that was obtained from LAMMPS was processed and handles using Jupyter Notebooks [28] coded in Python and using NumPy, pandas and SciPy [29]. OVITO has been used to visualize the results obtained from the simulations and to supply all the snapshots that have been reported in this work [30]. The results related to the temperature of the workpiece during the cutting process have been discussed in Sect. 4.1, and the forces experienced by the tool during the cutting process have been discussed in Sect. 4.2.

4.1 Analysis of Temperature During Machining

The temperature of the workpiece during the machining process for each rake angle simulated has been plotted in Fig. 2. As expected, the temperature of the workpiece increases monotonically as the DOC of the process is increased. Oscillations observed

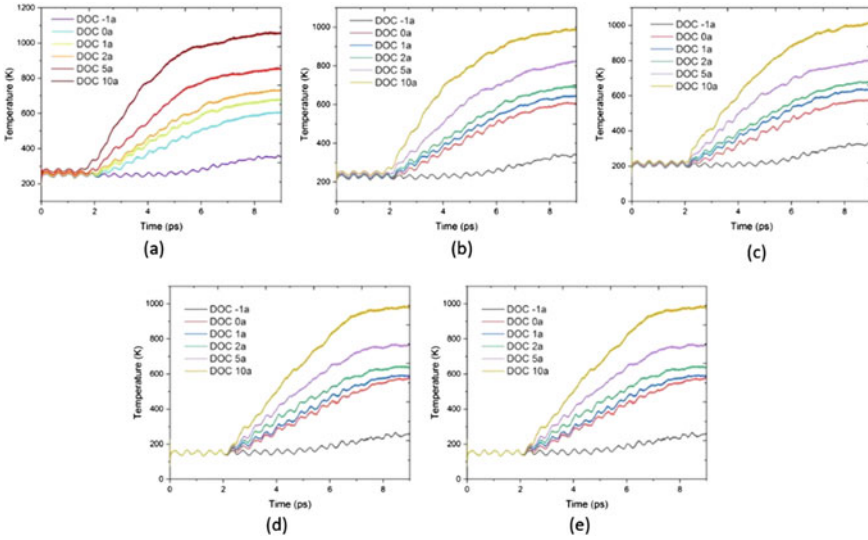


Fig. 2 Temperature of the workpiece for rake angles **a** -30° , **b** -15° , **c** 0° , **d** 15° and **e** 30°

in the plots are a common feature of the data obtained using MDS. The layer used to simulate the heat transfer of the region of cut with the bulk of the material is modeled using NVT ensemble. The NVT ensemble is used to define groups of atoms that conduct heat, but the velocity of the atoms is rescaled to keep the temperature of the system constant. The oscillations arise from the rescaling of the velocities of the atoms and have been observed in literature [9, 31]. The overall profile of the temperature with respect to time also agrees with the previous works. In addition to the profiles, we have also plotted data for the DOC of $-1a$. A negative depth of cut implies that the tool is not in cut but is simply gliding over the workpiece at a distance 1 atomic layer. This has been done to have an insight of the sensitivity of the interactions between the tool and the workpiece atoms. As far as the temperature is concerned, the interaction between the tool and workpiece when the tool is not in cut does not have much impact on the temperature of the process [18].

4.2 Analysis of Temperature During Machining

The force experienced by the tool of different rake angles with respect to time for different depths of cut is shown in figure Fig. 3. A plot for DOC $-1a$ have been added to the data for reasons similar to Fig. 2. Since the simulations are governed by potential functions this action itself (even when the tool is not in cut) would cause some force on the tool and the workpiece which has been plotted as DOC as $-1a$. As observed from the graphs, the force profile for the DOC as $-1a$ displays the same

profile for all rake angles and is hence also acts as a control for the experiments. It should be noted that large oscillations are observed in the force data obtained directly from LAMMPS. Hence, the data needs to be filtered before the presentation which has been accomplished using a moving average filter of window size 50. The scale of the oscillations has been reported in the graphs plotted by Goel et al. [8], where it can be seen that for small depth of cuts the oscillations can also cause the force to change the direction. The overall force profile is similar to the ones seen in the field of conventional manufacturing in the macro-domain. The force increases as the tool engages with the cut. There are oscillations similar to the oscillations cause in micro-machining due to chip breaking and then stabilizing while oscillating at a constant magnitude. However, it should be noted that in the simulations performed, no chip breakage was observed. The chip preferred to stick to the tool instead.

It was observed that among all the rake angles simulated, the forces with the -30° rake angle tool are most sensitive to the change in the depth of cut. This is as expected as the forces at DOC $0a$ are predominantly friction forces which are not expected to vary much with the DOC while the cutting forces are sensitive to the DOC. It was also observed that the forces for the higher rake angles are the most sensitive to the depth of cut. It can be hypothesized that while the positive rake angle of the tool removes material using a shearing process similar to macro-machining, the mechanism of cutting for negative rake angle tools tends to be extrusion [14]. It was also observed that on average, the tool with 0° experiences the least machining force. At a DOC of $0a$, the forces experienced by the various tools studied show a statistical range of $0.54\text{Ev}/\text{\AA}$ which increases to $2.15\text{Ev}/\text{\AA}$ for DOC $10a$. It observed that as the forces increase with the DOC, the average of the standard deviation remains

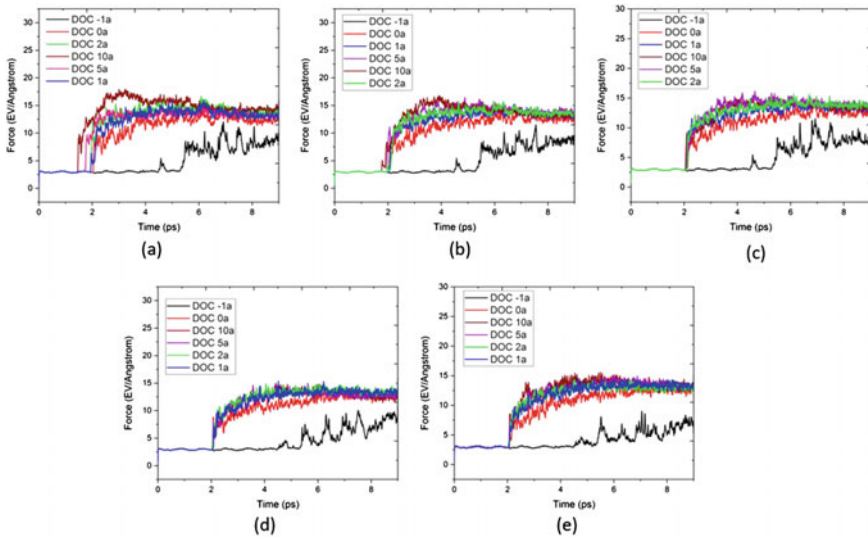


Fig. 3 Magnitude of force experienced by the tool for rake angles **a** -30° , **b** -15° , **c** 0° , **d** 15° and **e** 30°

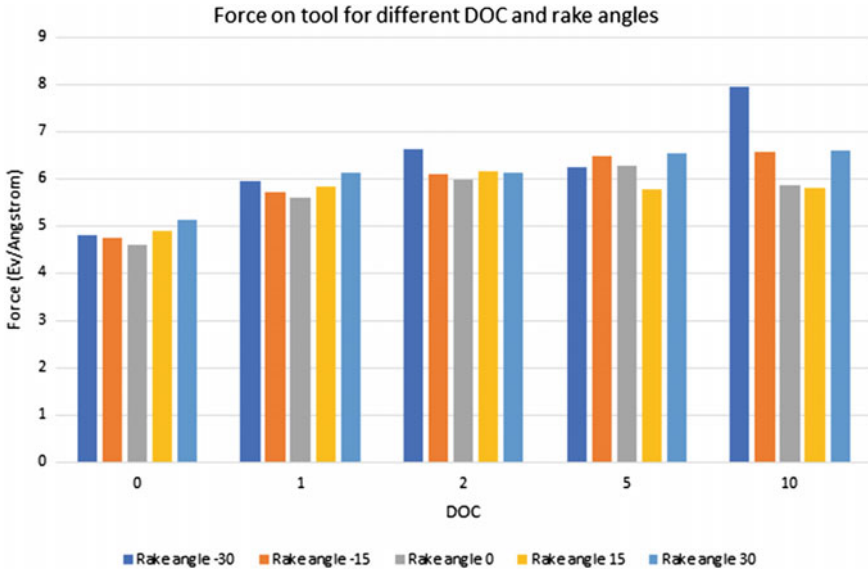


Fig. 4 Mean force experienced by tools (Y-axis) of different rake angles at different depths of cut (DOC) (X-axis)

fairly constant which indicated that the oscillations in the data are fairly constant. Compared to the neutral tool, the tool for rake angle -30° shows a $\approx 11.5\%$ increase in force, and the positive 30° rake angle tool shows a $\approx 7\%$ increase in force (Fig. 4).

5 Conclusions

The nanometric cutting process using single-point diamond cutting tool was simulated using LAMMPS. The temperature of the workpiece and the force experienced by the tool was observed. Tools for rake angle -30° , -15° , 0° , 15° and 30° were simulated, and the cutting process was observed for depths of cut $-1a$, $0a$, $1a$, $2a$, $5a$ and $10a$. It was observed that the tool for rake angle -30° was the most sensitive to change in the depth of cut in terms of the magnitude of force experienced. It was concluded that compared to a neutral rake angle, a negative rake angle can result in up to 11.5% increase in force, while a positive rake angle can result in up to 7.9% increase in force. Using negative rake angle, tools result in a greater heat evolution in the region of cut compared to +ve rake angle tool and the temperature increases monotonically with a decrease in the rake angle. The difference observed was 100 K from $+30^\circ$ to -30° .

References

1. Picard Y, Adams D, Vasile M, Ritchey M (2003) Focused ion beam-shaped microtools for ultra-precision machining of cylindrical components. *Precis Eng* 27(1):59–69
2. Tong Z, Luo X, Sun J, Liang Y, Jiang X (2015) Investigation of a scale-up manufacturing approach for nanostructures by using a nanoscale multi-tip diamond tool. *Int J Adv Manuf Technol* 80(1–4):699–710
3. Abraham MJ, Murtola T, Schulz R, Páll S, Smith JC, Hess B, Lindahl E (2015) GROMACS: high performance molecular simulations through multi-level parallelism from laptops to supercomputers. *SoftwareX* 1–2:19–25
4. Case DA, Darden TA, Cheatham TE, Simmerling CL, Wang J, Duke RE, Luo R, Crowley M, Walker RC, Zhang W (2008) Amber 10
5. Smith W, Forester TR, Todorov IT, Leslie M (2006) The DL poly 2 user manual. CCLRC, Daresbury Laboratory, Daresbury, Warrington WA4 4AD, England, vol 2
6. Plimpton S (1995) Fast Parallel algorithms for short-range molecular dynamics. *J Comput Phys* 117(1):1–19
7. Goel S, Haque Faisal N, Luo X, Yan J, Agrawal A (2014) Nanoindentation of polysilicon and single crystal silicon: molecular dynamics simulation and experimental validation. *J Phys D Appl Phys* 47(27):275304
8. Goel S, Luo X, Reuben RL (2013) Wear mechanism of diamond tools against single crystal silicon in single point diamond turning process. *Tribol Int* 57:272–281
9. Goel S, Luo X, Reuben RL, Pen H (2012) Influence of temperature and crystal orientation on tool wear during single point diamond turning of silicon. *Wear* 284–285:65–72
10. Mathews JA (1997) A silicon valley of the east: creating Taiwan's semiconductor industry. *Calif Manage Rev* 39(4):26–54
11. Shalf J (2020) The future of computing beyond Moore's Law. *Philos Trans Royal Soc A: Math Phy Eng Sci* 378(2166):20190061
12. Cai MB, Li XP, Rahman M (2007) Study of the mechanism of nanoscale ductile mode cutting of silicon using molecular dynamics simulation. *Int J Mach Tools Manuf* 47(1):75–80
13. Zhang P, Cao X, Zhang X, Wang Y (2021) Effects of cutting parameters on the subsurface damage of single crystal copper during nanocutting process. *Vacuum* 187:109420
14. Fang FZ, Wu H, Liu YC (2005) Modelling and experimental investigation on nanometric cutting of monocrystalline silicon. *Int J Mach Tools Manuf* 45(15):1681–1686
15. Ameli Kalkhoran SN, Vahdati M, Yan J (2019) Molecular dynamics investigation of nanometric cutting of single-crystal silicon using a blunt tool. *Jom* 71(12):4296–4304
16. Liu C, Zhang J, Zhang J, Chen X, He W, Xiao J, Xu J (2020) Influence of micro grooves of diamond tool on silicon cutting: a molecular dynamic study. *Mol Simul* 46(2):92–101
17. Lianfeng L, Qinchuan N, Minglin L (2020) Analysis of the influence of tool radius on mechanical state of monocrystalline silicon during nano-cutting. *Mech Adv Mater Struct* vol 0(0):1–15
18. Komanduri R, Raff LM (2001) A review on the molecular dynamics simulation of machining at the atomic scale. *Proc Inst Mech Eng Part B: J Eng Manuf* 215(12):1639–1672
19. Smit B (1992) Phase diagrams of Lennard-Jones fluids. *J Chem Phys* 96(11):8639–8640
20. Erhart P, Albe K (2005) Analytical potential for atomistic simulations of silicon, carbon, and silicon carbide. *Phys Rev B* 71(3):35211
21. Girifalco LA, Weizer VG (1959) Application of the morse potential function to cubic metals. *Phys Rev* 114(3):687
22. Becquart CS, Decker KM, Domain C, Ruste J, Souffez Y, Turbatte JC, Van Duysen JC (1997) Massively parallel molecular dynamics simulations with EAM potentials. *Radiat Eff Defects Solids* 142(1–4):9–21
23. Tersoff J (1986) New Empirical model for the structural properties of silicon. *Phys Rev Lett* 56(6):632–635
24. Tersoff J (1994) Chemical order in amorphous silicon carbide. *Phys Rev B* 49(23):16349–16352

25. Komanduri R, Chandrasekaran N, Raff LM (1999) Orientation effects in nanometric cutting of single crystal materials: an MD simulation approach. *CIRP Ann Manuf Technol* 48(1):67–72
26. Van Gunsteren WF, Berendsen HJC (1988) A leap-frog algorithm for stochastic dynamics. *Mol Simul* 1(3):173–185
27. Grubmüller H, Heller H, Windemuth A, Schulten K (1991) Generalized verlet algorithm for efficient molecular dynamics simulations with long-range interactions. *Mol Simul* 6(1–3):121–142
28. Kluyver T, Ragan-Kelley B, Pérez F, Granger B, Bussonnier M, Frederic J, Kelley K, Hamrick J, Grout J, Corlay S, Ivanov P, Avila D, Abdalla S, Willing C (2016) Jupyter notebooks—a publishing format for reproducible computational workflows. Positioning and power in academic publishing: players, agents and agendas. Loizides F, Schmidt B (eds)
29. McKinney W (2010) Data structures for statistical computing in python. In: Proceedings of the 9th python in science conference. Van der Walt S, Millman J (eds)
30. Stukowski A (2010) Visualization and analysis of atomistic simulation data with OVITO—the open visualization tool. *Model Simul Mater Sci Eng* (1)
31. Chavoshi SZ, Goel S, Luo X (2016) Influence of temperature on the anisotropic cutting behaviour of single crystal silicon: a molecular dynamics simulation investigation. *J Manuf Process* 23:201–210